



# An improved polygon mesh generation and its application in SBFEM using NURBS boundary

Xinqing Li<sup>1</sup> · Hailiang Su<sup>1,2</sup> · Yingjun Wang<sup>1</sup>

Received: 21 February 2024 / Accepted: 18 May 2024 / Published online: 17 June 2024  
© The Author(s), under exclusive licence to Springer-Verlag GmbH Germany, part of Springer Nature 2024

## Abstract

Aiming to address the challenge of inaccurately describing the curve boundary of the complex design domain in traditional finite element mesh, this paper proposes an improved polygon mesh generation and polygon scaled boundary finite element method (PSBFEM) using non-uniform rational B-spline (NURBS) boundary. In the improved mesh generation scheme, the domain boundary will be accurately described using NURBS curves. Within this framework, a NURBS updating strategy is proposed, allowing the NURBS curve information on the boundary to be updated as the mesh changes. By employing point inversion and knot insertion, additional control points are introduced to ensure that some coincide with the nodes of the elements, thereby guaranteeing the accuracy of subsequent analyses. The boundary elements can be discretized into NURBS elements and conventional elements using SBFEM, whose physical fields are respectively constructed using NURBS basis functions and Lagrange shape functions in the circumferential direction. In the radial direction, by transforming a system of partial differential equations into a system of ordinary differential equations, which can be analytically solved without fundamental solutions. Furthermore, the internal elements can be solved directly with the traditional polygon SBFEM. The numerical examples demonstrate that the proposed method can achieve a high-quality polygon mesh with NURBS updating. Moreover, it effectively solves the corresponding polygon elements and significantly improves the accuracy of the displacement and stress solutions compared to the traditional polygon SBFEM.

**Keywords** NURBS boundary · Polygon mesh · SBFEM · Complex design domain

## 1 Introduction

The finite element method (FEM), as a crucial approach for solving partial differential equations, finds extensive application in numerical simulations across engineering and various other fields. However, the conventional employment of triangular and quadrilateral elements in the finite element method often poses challenges when describing complex models'

boundaries. Conversely, employing complex polygon elements offers evident advantages [1], such as greater flexibility for the meshing of complex geometries, and more effective simulation of mechanical properties. Common polygon meshes are usually generated by Delaunay triangulation [2, 3] or Voronoi diagrams [4, 5]. The primary challenge in utilizing polygon elements within the FEM lies in constructing polynomial interpolation functions of physical fields that satisfies the coordination of elements [6]. Various solutions have been proposed to address this issue, including Wachspress interpolation [7, 8], Laplace interpolation [9, 10], and mean value coordinates [11, 12].

Wolf and Song [13] pioneered a semi-analytical and semi-numerical method for solving partial differential equations, known as the scaled boundary finite element method (SBFEM). This method can realize the boundary discretization and combines the advantages of FEM and boundary element method (BEM), exhibiting characteristics such as reduced computational dimension and elimination of the need for fundamental solutions, thereby enabling efficient

✉ Yingjun Wang  
wangyj84@scut.edu.cn

<sup>1</sup> National Engineering Research Center of Novel Equipment for Polymer Processing, The Key Laboratory of Polymer Processing Engineering of the Ministry of Education, Guangdong Provincial Key Laboratory of Technique and Equipment for Macromolecular Advanced Manufacturing, South China University of Technology, Guangzhou 510641, China

<sup>2</sup> School of Mechanical and Automotive Engineering, Guangxi University of Science and Technology, Liuzhou 545006, China

and accurate numerical computations. The application of SBFEM was subsequently extended by Ooi et al. [14] to encompass polygons with any number of sides, thereby significantly enhancing the accuracy and efficiency of the solution. Geometric shapes only needs to satisfy the scaling conditions required by SBFEM [15], a criterion that makes SBFEM an ideal platform for developing polygon-based shape functions. Furthermore, polygon meshes can be conveniently constructed as dual meshes of triangular meshes [16], facilitating their extensive utilization in the SBFEM and rendering it comparable to the traditional FEM in terms of applicability. The Polygon SBFEM (PSBFEM) was initially used to solve fracture problems [17, 18]. Due to its shape function containing singular terms, which can be directly obtained in the solving process of SBFEM elements [19], the SBFEM can simplify the solution of singular problems and enhance calculation accuracy. In addition, PSBFEM has been successfully applied into various fields including Elasto-plasticity [20], Vibration Analysis [21], Seepage Problems [22], Dynamic analyses [23]. Although the development of PSBFEM has significantly enhanced solution efficiency and accuracy, it still falls short in accurately describing the boundary of complex design domains.

The emergence of isogeometric analysis (IGA) [24] offers an alternative approach for solution of accurate geometry. In contrast to the Lagrange basis function employed in traditional FEM, IGA direct uses exact geometric spline basis functions in analysis, e.g., NURBS [25], hybrid B-splines [26], T-splines [27] and PHT splines [28], which achieves high continuity between elements. As a widely-used technique for representing curves, NURBS can be constructed through B-splines. A knot vector of B-splines, denoted by  $\Xi = [\eta_0, \eta_1, \dots, \eta_{n+p}]$ , consists of a non-decreasing real number sequence in the parameter space, where  $n$  is the number of control points,  $p$  represents the order of the spline. The basis function  $N_{i,p}(\eta)$  of B-spline can be defined by Cox-de Boor recursion formula [29] as

$$N_{i,0}(\eta) = \begin{cases} 1, & \text{if } \eta_i \leq \eta < \eta_{i+1} \\ 0, & \text{Otherwise} \end{cases}$$

$$N_{i,p}(\eta) = \frac{(\eta - \eta_i)N_{i,p-1}(\eta)}{\eta_{i+p} - \eta_i} + \frac{(\eta_{i+p+1} - \eta)N_{i+1,p-1}(\eta)}{\eta_{i+p+1} - \eta_{i+1}}$$

(1)

if  $\eta_i \leq \eta < \eta_{i+1}$

By introducing a positive weight  $\omega$ , the NURBS basis function can be rationalized by B-splines as

$$R_{i,p}(\eta) = \frac{N_{i,p}(\eta)\omega_i}{\sum_j^n N_{j,p}(\eta)\omega_j}$$

(2)

The corresponding NURBS curve can be expressed as

$$S(\eta) = \sum_{i=0}^n R_{i,p}(\eta)P_i$$

(3)

where  $P$  represents the control points of the NURBS curve. In recent years, the combination of IGA and SBFEM has received great deal of attentions by numerous researchers to further enhance calculation accuracy. Zhang and Lin [30, 31] firstly proposed a scaled boundary isogeometric analysis (SBIGA), which employed NURBS for describing the boundary of SBFEM, to achieve accurate solution. Gravenkamp et al. [32] extensively revisited the utilization of higher-order shape functions such as NURBS in SBFEM. Zang et al. [33, 34] proposed a NURBS-Enhanced PSBFEM to solve heat diffusion and developed a polygonal scaled boundary isogeometric method for 2D elasticity problems involving trimmed geometries. References [35–38] further discussed the application of NURBS-based SBFEM in practical problems. A majority of these studies, however, heavily rely on manual NURBS patches settings or initial NURBS information such as specifying initial control points to coincide with element nodes. Undoubtedly, this will lead to challenges in dealing with complex design domain issues. Recently, a NURBS-boundary-based SBFEM [39] have been proposed under the quadtree framework, which employ the NURBS to describe domain's boundary for subsequent analysis. The adoption of quadtree meshes greatly enhances computational efficiency, but there is still room for improvement in terms of solution accuracy.

Klinkel et al. [40] proposed a NURBS-based hybrid collocation-Galerkin method for 2D plane-stress elastic problems, which effectively combines the advantages of SBFEM and isogeometric collocation methods. Later, Klinkel and Reichel [41] presented a finite element formulation in boundary representation for the analysis of nonlinear problems by means of scaling approach, then they [42] developed NURBS-enhanced finite element formulations based on scaled boundary parameterization within polygon mesh framework. These methods introduce the boundary scaling technique adopted from SBFEM, combined with the concept of isogeometric analysis, greatly enhancing the accuracy of the solution. In comparison to the aforementioned method, this study proposes an improved NURBS-based polygon mesh generation scheme that NURBS information can be updated along with the changes in the polygon mesh. Under the initial NURBS, the knot vector corresponding to the intersection points of the boundary curves and polygon meshes is obtained through point inversion, followed by knot insertion to achieve updating of NURBS. This ensures that the control points of NURBS fall precisely at the intersection positions, facilitating subsequent accurate solutions. Additionally, we propose a NURBS-boundary-based polygon

scaled boundary finite element method (NPSBFEM) tailored for the improved polygon mesh. This method effectively integrates the advantages of PSBFEM and SBIGA, with the core still rooted in SBFEM. For the internal elements in the problem domain, direct calculations will be performed using PSBFEM. The focus lies on the elements along the boundaries. By employing the dimension reduction capability of SBFEM, boundary meshes will be discretized into NURBS curve elements and Lagrange line elements. For NURBS curve elements, the SBIGA will be utilized to obtain their coefficient matrices. Simultaneously, for Lagrange line elements, the approach of PSBFEM will be applied to acquire their coefficient matrices. Subsequently, coefficient matrices will be assembled to solve the scaled boundary finite element equations.

The remaining sections of this paper are outlined as follows: Sect. 2 introduces the generation process of novel polygon mesh. Section 3 presents the NURBS updating strategy to precisely impose control points. Section 4 elaborates on the implementation process of NPSBFEM. Numerical examples are presented in Sect. 5 to demonstrate the effectiveness of the proposed mesh and method. Finally, in Sect. 6, brief conclusions are provided highlighting the key points discussed in this paper.

## 2 Polygon mesh generation of NURBS boundary description

The present work proposes a novel scheme for generating polygon meshes using spline boundary description and Delaunay triangulation. Distmesh [43], a simple mesh generator in MATLAB, is utilized to generate unstructured triangular meshes. However, this mesh fails to accurately represent the design domain's boundary, leading to inevitable solution errors. Moreover, an excessive number of triangular meshes increases the degree of freedom and subsequently escalates computational costs. To address these issues, transforming the triangular meshes into a polygon mesh [14] provides a viable solution that not only accommodates complex design domains but also simplifies the problem-solving process. Nevertheless, constructing boundary meshes by connecting midpoint boundaries weakens solution accuracy. In contrast, employing NURBS to describe the design domain's boundary enables us to overcome these aforementioned challenges.

CAD software can be utilized in the structural design domain to acquire NURBS information of the domain boundary, including control points, knot vector, and weights. This information is then combined with polygon mesh generation to construct a mesh generation scheme using spline description, as depicted in Fig. 1.

The specific steps for implementation are as follows.

Step 1: Utilizing Rhino software to acquire the control points and other pertinent information of the design domain boundary.

Step 2: Triangulating the design domain to obtain essential data such as vertex, centroid, and boundary midpoint information for each triangulation element.

Step 3: Combining the initial NURBS information with the boundary midpoint of the external triangular element to update the spline curve. Refer to Sect. 3 for detailed instructions.

Step 4: Constructing a polygon mesh by connecting triangle centroids for inner elements, while outer elements are initially formed by connecting centroids, vertices, and midpoints of boundary triangles.

Step 5: Substituting boundaries of external elements obtained in step 4 with NURBS curves acquired in Step 3 to create the desired polygon mesh. It should be noted that control points of updated NURBS curves can coincide with boundary nodes of external elements for ease in subsequent accurate solutions.

## 3 NURBS updating scheme of polygon mesh

In this section, a NURBS updating scheme is proposed to meet the subsequent solution requirements of the polygon mesh. The core of this scheme lies in the utilization of point inversion and knot insertion techniques to obtain new NURBS information, ensuring that boundary nodes have corresponding control points to fulfill the boundary discretization requirements of SBFEM.

### 3.1 Polygon scaled boundary element

For a design domain with complex boundaries, Fig. 2a demonstrates the representation of traditional PSBFEM with linear connection at the nodes, which inevitably affects the accuracy of solution. As mentioned in Sect. 2, NURBS boundary is employed to accurately describe the design domain boundary in this work. The schematic diagram of quadratic SBFEM polygon mesh using NURBS boundaries is depicted in Fig. 2b, where the polygon elements in two dimensions based on SBFEM are termed S-elements [16]. Within each S-element, a local coordinate system  $(\xi, \eta)$  is established at a point known as the scaling center  $O$  from which the entire boundary is visible. Herein,  $\eta$  represents the tangential coordinates and can be utilized for constructing the NURBS parameter space, and  $\xi$  denotes the radial coordinates. Specifically,  $\xi$  equals 0 at the scaling center and 1 at the element boundary.

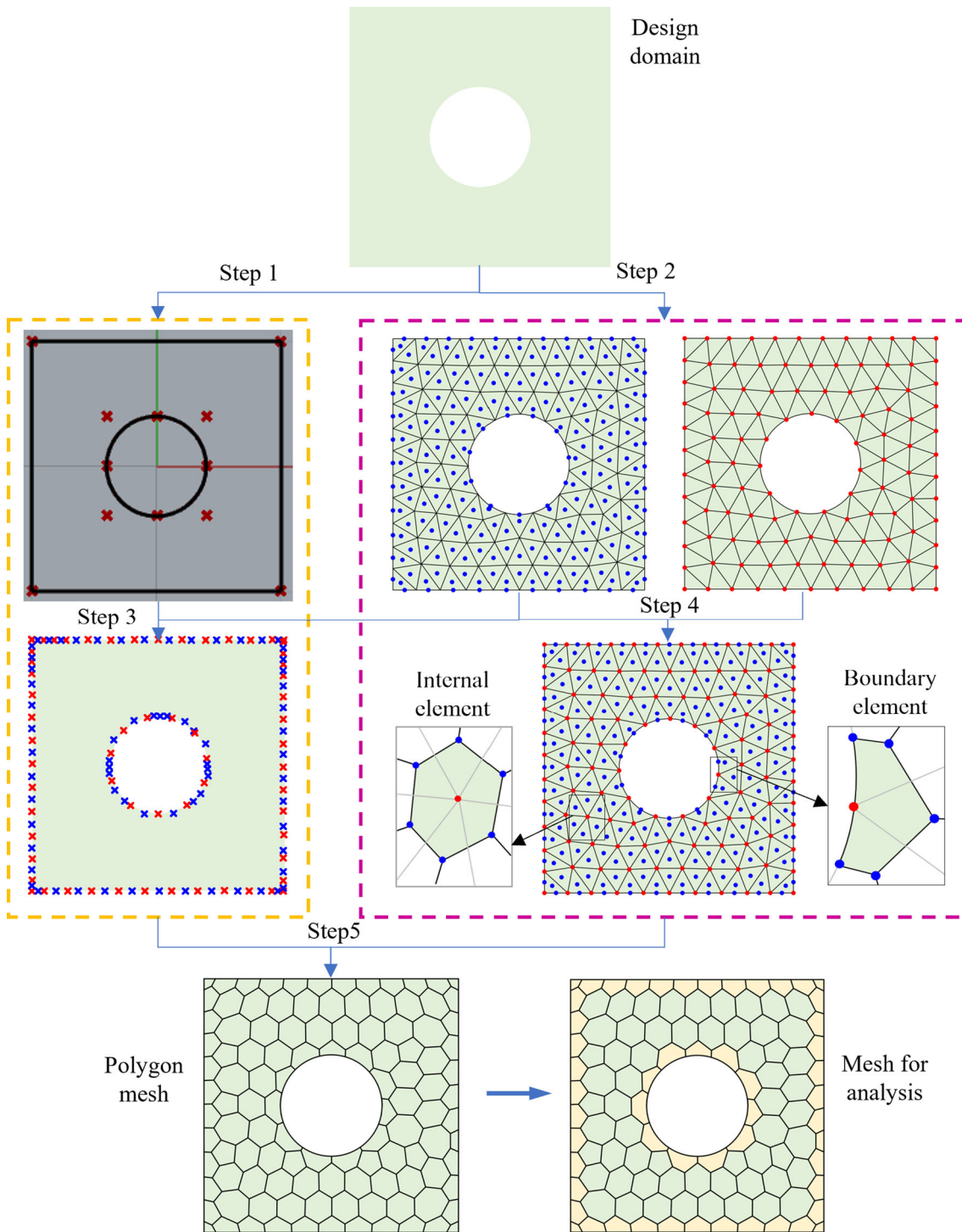


**Fig. 1** Polygon mesh generation scheme of spline boundary description based on Delaunay triangulation

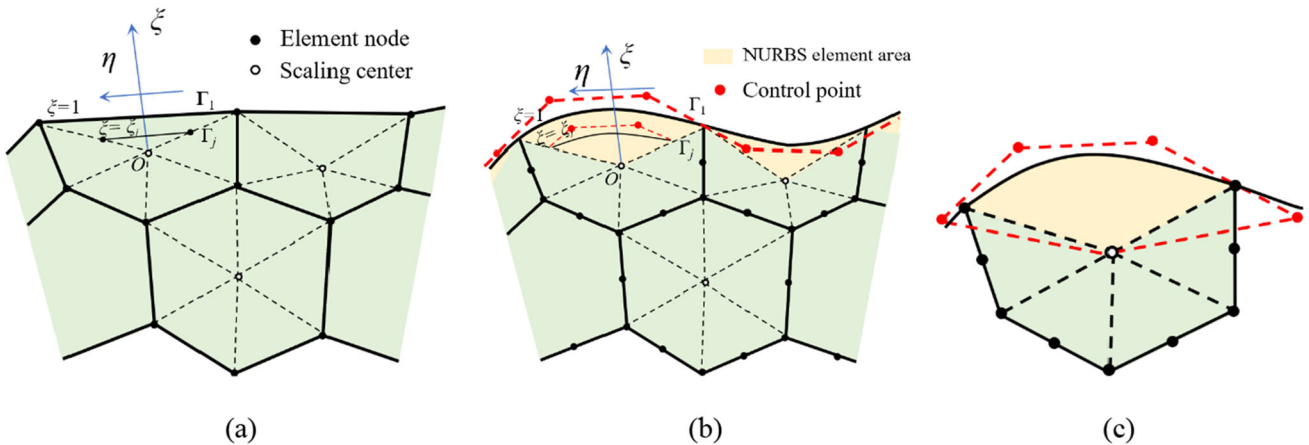


**Fig. 2** Polygon scaled boundary element, **a** linear element, **b** quadratic element with NURBS boundary, **c** boundary element

### 3.2 Strategy for NURBS updating

Notably, when dealing with complex design domain structure, it often becomes challenging to precisely impose control points. For polygon elements with NURBS boundaries, let's take the boundary element shown in Fig. 2c of this paper as an example. When the control points are not on the boundary and do not coincide with the element nodes, the necessary condition for boundary discretization, i.e., continuity of displacement at the end nodes where the elements are connected, cannot be met. Consequently, it fails to meet the necessary condition for boundary discretization, thus rendering it unsuitable for subsequent computation using SBFEM. Based on this observation, we propose a NURBS updating strategy to precisely impose control points. By employing point inversion and knot insertion techniques, we determine the parameter values corresponding to the boundary nodes from given initial NURBS information and achieve accurate imposition of control points.

The determination of the parameter value  $\bar{\eta}$  corresponding to the boundary node coordinate  $\mathbf{P}_{\text{ins}} = (x, y, z)$  (i.e.  $\mathbf{S}(\bar{\eta}) = \mathbf{P}_{\text{ins}}$ ) is referred to as the point inversion. The process can be divided into three steps. Firstly, by leveraging the strong convex hull property of NURBS, we can determine the spans of curve  $\mathbf{S}(\eta)$  that may encompass node  $\mathbf{P}_{\text{ins}}$ . Then, through the utilization of knot refinement or insertion techniques, these identified spans are transformed into power basis form. Finally, for each span, a set of three polynomial equations with unknown parameters is established, and if these equations possess a common solution, it indicates that  $\mathbf{P}_{\text{ins}}$  lies on the curve.

Assuming a span  $c(\eta) = \mathbf{a}_0^\omega + \mathbf{a}_1^\omega \eta + \mathbf{a}_2^\omega \eta^2$  of NURBS can be represented as a vector function, where  $\mathbf{a}_i^\omega = (\omega_i x_i, \omega_i y_i, \omega_i z_i, \omega_i)$ . By projecting this span into three-dimensional space and equating it to  $\mathbf{P}_{\text{ins}}$ , the following equation is obtained

$$\begin{cases} \frac{\omega_2 x_2 \eta^2 + \omega_1 x_1 \eta + \omega_0 x_0}{\omega_2 \eta^2 + \omega_1 \eta + \omega_0} = x \\ \frac{\omega_2 y_2 \eta^2 + \omega_1 y_1 \eta + \omega_0 y_0}{\omega_2 \eta^2 + \omega_1 \eta + \omega_0} = y \\ \frac{\omega_2 z_2 \eta^2 + \omega_1 z_1 \eta + \omega_0 z_0}{\omega_2 \eta^2 + \omega_1 \eta + \omega_0} = z \end{cases} \quad (4)$$

which yields

$$\begin{cases} \omega_2(x_2 - x)\eta^2 + \omega_1(x_1 - x)\eta + \omega_0(x_0 - x) = 0 \\ \omega_2(y_2 - y)\eta^2 + \omega_1(y_1 - y)\eta + \omega_0(y_0 - y) = 0 \\ \omega_2(z_2 - z)\eta^2 + \omega_1(z_1 - z)\eta + \omega_0(z_0 - z) = 0 \end{cases} \quad (5)$$

The main focus of this paper is exclusively on the 2D scenario, assuming  $z = 0$ . Additionally, we elegantly employ the Newton iteration method to minimize the distance between the node  $\mathbf{P}_{\text{ins}}$  and the NURBS curve  $\mathbf{S}(\eta)$ .

Given an initial value  $\eta_0$ , the dot product is defined as

$$f(\eta) = \mathbf{S}'(\eta)(\mathbf{S}(\eta) - \mathbf{P}_{\text{ins}}) \quad (6)$$

when  $f'(\eta) = 0$ , the distance from the point  $\mathbf{P}_{\text{ins}}$  to  $\mathbf{S}(\eta)$  is minimized. The point is deemed to lie on the curve if the minimum distance falls below a pre-specified precision. Let  $\eta_i$  denotes the parameter value obtained in the  $i$ -th iteration.

$$\eta_{i+1} = \eta_i - \frac{f(\eta_i)}{f'(\eta_i)} = \eta_i - \frac{\mathbf{S}'(\eta_i)(\mathbf{S}(\eta_i) - \mathbf{P}_{\text{ins}})}{\mathbf{S}''(\eta_i)(\mathbf{S}(\eta_i) - \mathbf{P}_{\text{ins}}) + |\mathbf{S}'(\eta_i)|^2} \quad (7)$$

The convergence can be indicated by employing two zero tolerances, and the criteria for convergence are as follows

$$\begin{aligned} |(\eta_{i+1} - \eta_i)\mathbf{S}'(\eta)| &\leq \chi_1 \\ |\mathbf{S}(\eta) - \mathbf{P}_{\text{ins}}| &\leq \chi_1 \\ \frac{|\mathbf{S}'(\eta)(\mathbf{S}(\eta) - \mathbf{P}_{\text{ins}})|}{|\mathbf{S}'(\eta)| |\mathbf{S}(\eta) - \mathbf{P}_{\text{ins}}|} &\leq \chi_2 \end{aligned} \quad (8)$$

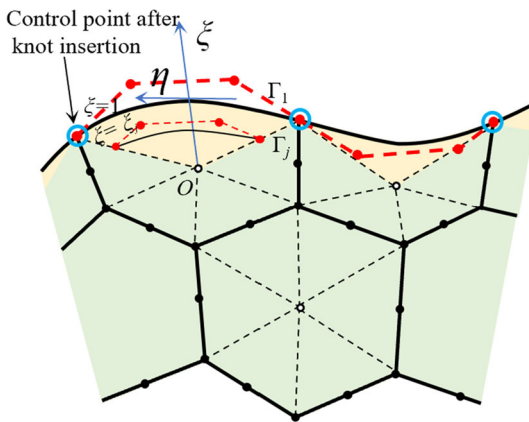


**Fig. 3** Quadratic SBFEM polygon meshes using NURBS boundaries after knot insertion

where,  $\chi_1$  and  $\chi_2$  respectively represent whether the measures of Euclidean distance and cosine distance are equal to 0.

Subsequently, it is necessary to incorporate parameter value  $\bar{\eta}$  into the existing knot vector  $\Xi$  to construct a new knot vector  $\bar{\Xi} = [\bar{\eta}_0 = \eta_0, \dots, \bar{\eta}_k = \eta_k, \bar{\eta}_{k+1} = \bar{\eta}]$ . The updated NURBS curve is represented as

$$\bar{S}(\eta) = \sum_{i=0}^{n+1} \bar{R}_{i,p}(\eta) Q_i \quad (9)$$

where  $\bar{R}_{i,p}$  represents the new basis function on the knot vector  $\bar{\Xi}$ ,  $Q_i$  denotes the new control point, which is defined as

$$Q_i = \alpha_i P_i + (1 - \alpha_i) P_{i-1}, \quad \alpha_i = \begin{cases} 1, & i \leq k-p \\ \frac{\bar{\eta} - \eta_i}{\bar{\eta}_{i+p} - \bar{\eta}_i}, & k-p+1 \leq i \leq k \\ 0, & i \geq k+1 \end{cases} \quad (10)$$

Notably that when a node on the boundary connects two elements, knot insertion will be performed twice at this specific location. Consequently, duplicate knots will occur, resulting in the control points being imposed precisely on the boundary nodes. Figure 3 displays the quadratic SBFEM polygon mesh using NURBS boundaries after knot insertion. It can be observed that the control points are accurately imposed onto the elements for subsequent accurate solution.

## 4 NURBS-boundary-based polygon SBFEM

### 4.1 Elastostatic problem

This work focuses on the elastostatic problem, which is a typical boundary value problem in mechanics analysis.

It is described by three governing equations: the equilibrium equation, strain-displacement equation, and constitutive equation

$$L^T \sigma + \bar{f} = 0 \quad (11)$$

$$\sigma = D \epsilon \quad (12)$$

$$\epsilon = L u \quad (13)$$

where  $L$  represents differential operator,  $\sigma$  is stress vector,  $\bar{f}$  is volume force vector.  $D$  represents the elastic matrix and  $u$  is the displacement vector. And two sets of boundary conditions: displacement boundary condition and force boundary condition.

### 4.2 Solution of boundary polygon element stiffness matrix

The fundamental principles and coordinate transformations of SBFEM have been extensively discussed by Wolf and Song [44, 45], while this section provides only a concise overview. For a design domain with complex boundaries, NURBS can be employed to discretize the domain boundary. Furthermore, the boundary element of polygon mesh using NURBS boundaries can be regarded as an S-element. Within the framework of PSBFEM, S-elements are discretized into NURBS element and quadratic elements, as depicted in Fig. 4. The only requirement for boundary discretization is to ensure displacement continuity at the connecting node of each element, this condition can be effectively met by NURBS updating strategy mentioned in Sect. 3.2.

The domain boundary is discretized by NURBS, and the boundary elements are further divided into NURBS elements and quadratic elements. The former utilizes NURBS basis functions for coordinate transformation, thereby converting the Cartesian coordinates of the control points to scaled boundary coordinates.

$$\begin{aligned} \hat{x}(\xi, \eta) &= x_0 + \xi R(\eta)x \\ \hat{y}(\xi, \eta) &= y_0 + \xi R(\eta)y \end{aligned} \quad (14)$$

where  $(\hat{x}, \hat{y})$  denotes arbitrary point coordinate in the domain,  $(x_0, y_0)$  and  $(x, y)$  denote the coordinate of scaling center and control points, respectively.

The concept of isoparametric is employed to approximate the displacement field variable  $u$  of the boundary region.

$$u(\xi, \eta) = R_n(\eta)u(\xi) \quad (15)$$

where  $R_n$  represents the interpolation functions which are applied to each DOF of an element separately by means of multiplication with the identity matrix  $I_{2 \times 2}$ , defined as

**Fig. 4** The boundary element of polygon mesh using NURBS boundary

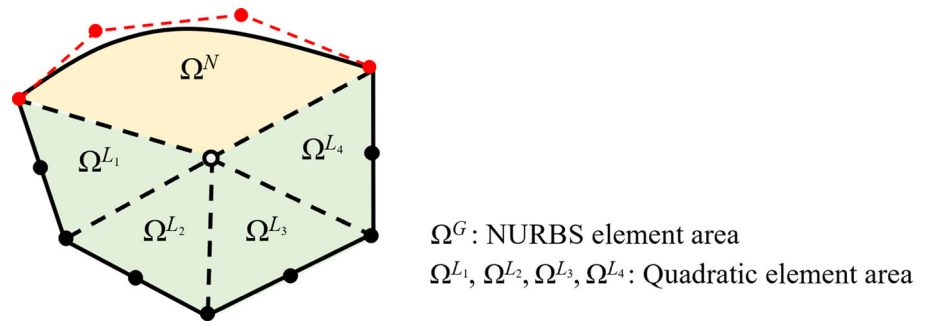
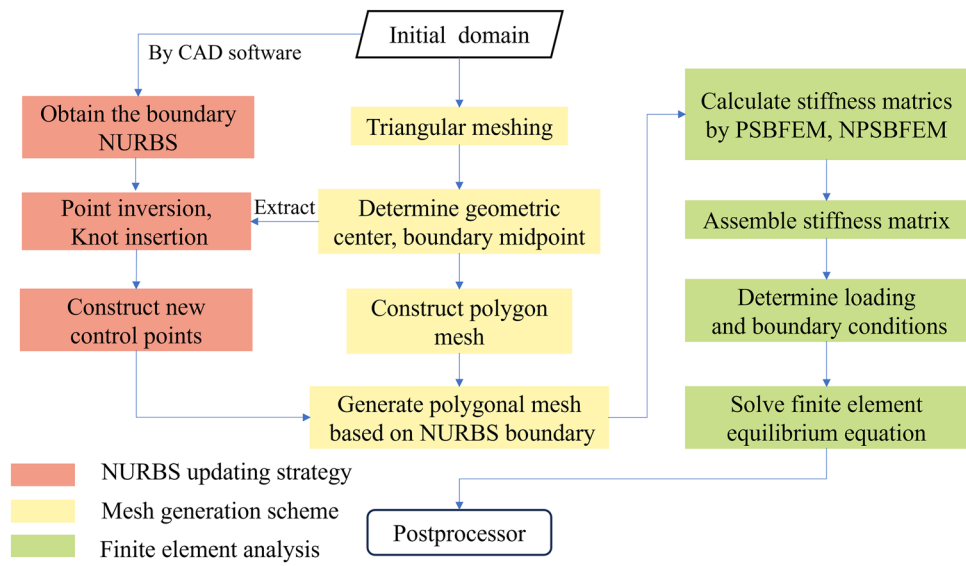


**Fig. 5** The flowchart of NPSBFEM implementation under 2D elastostatic problem



$$\mathbf{R}_n = [R_{i,p} \mathbf{I}_{2 \times 2} R_{i+1,p} \mathbf{I}_{2 \times 2} R_{i+2,p} \mathbf{I}_{2 \times 2}] \quad (16)$$

Currently, the PSBFEM has traditionally utilized Lagrange shape functions up to order 3 [46], with nodes uniformly distributed in the local element coordinate system. In this paper, we only consider the case of order 1 and order 2 for comparison with NURBS. For a 2-noded linear element, its Lagrange shape functions can be expressed as

$$\begin{aligned} N_{L_0} &= (1 - \eta)/2 \\ N_{L_1} &= (1 + \eta)/2 \end{aligned} \quad (17)$$

The corresponding interpolation function is

$$\mathbf{N}_L = [N_{L_0} \mathbf{I}_{2 \times 2} N_{L_1} \mathbf{I}_{2 \times 2}] \quad (18)$$

For quadratic element, the corresponding Lagrange shape functions are

$$\begin{aligned} N_{L_0} &= \eta(\eta - 1)/2 \\ N_{L_1} &= (1 + \eta)(1 - \eta) \\ N_{L_2} &= \eta(\eta + 1)/2 \end{aligned} \quad (19)$$

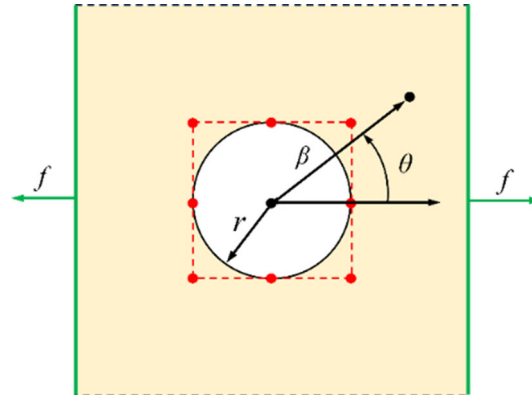


**Fig. 6** Infinite plane with hole

The interpolation function is defined as

$$\mathbf{N}_L = [N_{L_0} \mathbf{I}_{2 \times 2} N_{L_1} \mathbf{I}_{2 \times 2} N_{L_2} \mathbf{I}_{2 \times 2}] \quad (20)$$

Subsequently, the stress field of NURBS element area can be mathematically expressed

$$\boldsymbol{\sigma}(\xi, \eta) = \mathbf{D}\boldsymbol{\epsilon}(\xi, \eta) = \mathbf{D} \left( \mathbf{B}_1 \mathbf{u}(\xi), \xi + \frac{1}{\xi} \mathbf{B}_2 \mathbf{u}(\xi) \right) \quad (21)$$

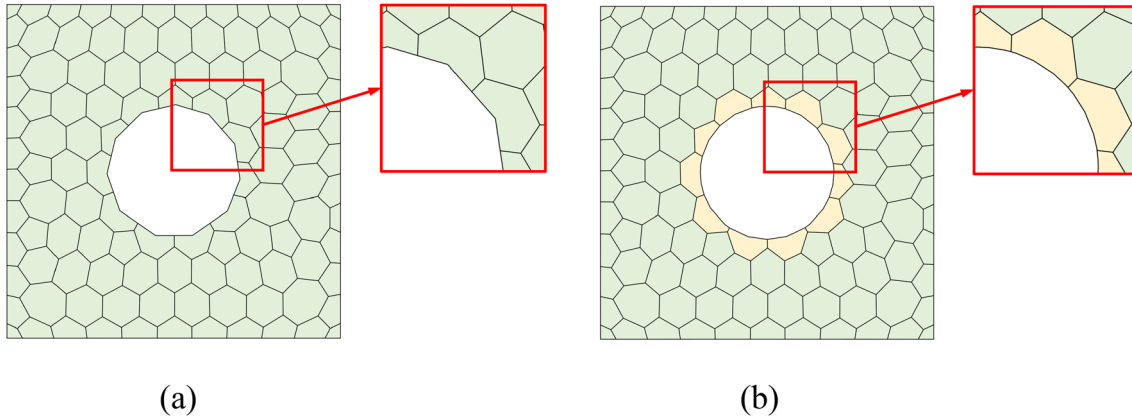


**Fig. 7** Polygon mesh generation, **a** Distmesh-based, **b** NURBS-boundary-based

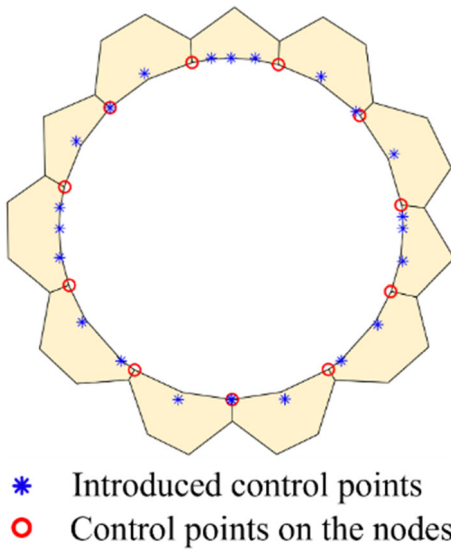


**Fig. 8** Updated control points

where  $\mathbf{B}_1$  and  $\mathbf{B}_2$  denote the correlation between strain and displacement, which are defined as

$$\begin{aligned} \mathbf{B}_1 &= \mathbf{b}_1 \mathbf{R}_n \\ \mathbf{B}_2 &= \mathbf{b}_2 \mathbf{R}_{n,\eta} \end{aligned} \quad (22)$$

and

$$\begin{aligned} \mathbf{b}_1(\eta) &= \frac{1}{|\mathbf{J}|} \begin{bmatrix} \hat{y}(\eta), \eta & 0 \\ 0 & -\hat{x}(\eta), \eta \\ -\hat{x}(\eta), \eta & \hat{y}(\eta), \eta \end{bmatrix} \\ \mathbf{b}_2(\eta) &= \frac{1}{|\mathbf{J}|} \begin{bmatrix} -\hat{y}(\eta) & 0 \\ 0 & \hat{x}(\eta) \\ \hat{x}(\eta) & -\hat{y}(\eta) \end{bmatrix} \end{aligned} \quad (23)$$

where  $\mathbf{J}$  is the Jacobian matrix

$$\mathbf{J} = \begin{bmatrix} \hat{x}(\eta) & \hat{y}(\eta) \\ \hat{x}(\eta), \eta & \hat{y}(\eta), \eta \end{bmatrix} \quad (24)$$

By substituting the above coordinate transformation into the virtual work principle, the control partial differential equation can be transformed into a set of second-order ordinary differential equations about the scaled boundary coordinates  $\xi$ , namely, the scaled boundary finite element equations

$$\mathbf{E}_0 \xi^2 \mathbf{u}(\xi), \xi \dot{\xi} + (\mathbf{E}_0 + \mathbf{E}_1^T - \mathbf{E}_1) \xi \mathbf{u}(\xi), \xi - \mathbf{E}_2 \mathbf{u}(\xi) = 0 \quad (25)$$

where  $\mathbf{E}_0$ ,  $\mathbf{E}_1$  and  $\mathbf{E}_2$  can be referred as coefficient matrix, defined as follows

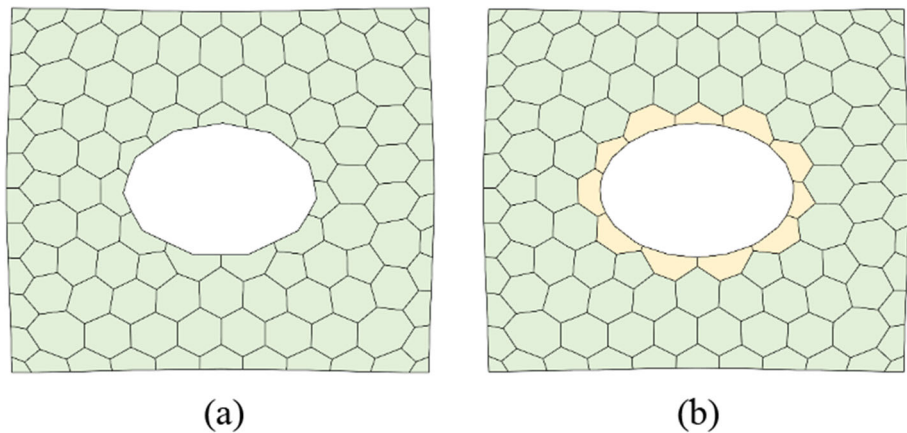
$$\begin{aligned} \mathbf{E}_0 &= \int_{\partial\Omega^N} \mathbf{B}_1(\eta)^T \mathbf{D} \mathbf{B}_1(\eta) |\mathbf{J}| d\eta + \int_{\partial\Omega^L} \mathbf{B}_1^L(\eta)^T \mathbf{D} \mathbf{B}_1^L(\eta) |\mathbf{J}^L| d\eta \\ \mathbf{E}_1 &= \int_{\partial\Omega^N} \mathbf{B}_2(\eta)^T \mathbf{D} \mathbf{B}_1(\eta) |\mathbf{J}| d\eta + \int_{\partial\Omega^L} \mathbf{B}_2^L(\eta)^T \mathbf{D} \mathbf{B}_1^L(\eta) |\mathbf{J}^L| d\eta \\ \mathbf{E}_2 &= \int_{\partial\Omega^N} \mathbf{B}_2(\eta)^T \mathbf{D} \mathbf{B}_2(\eta) |\mathbf{J}| d\eta + \int_{\partial\Omega^L} \mathbf{B}_2^L(\eta)^T \mathbf{D} \mathbf{B}_2^L(\eta) |\mathbf{J}^L| d\eta \end{aligned} \quad (26)$$

where  $\Omega^N$  and  $\Omega^L$  represent NURBS and line element areas, respectively.  $\mathbf{B}_1^L$  and  $\mathbf{B}_2^L$  respectively denote the correlation between strain and displacement of the Lagrange,  $\mathbf{J}^L$  is the Jacobian matrix of the Lagrange.

To solve Eq. 15, first transform the equation into a first-order differential equation

$$\xi \left\{ \begin{array}{l} \mathbf{u}(\xi) \\ \mathbf{q}(\xi) \end{array} \right\}_{,\xi} = \mathbf{Z} \left\{ \begin{array}{l} \mathbf{u}(\xi) \\ \mathbf{q}(\xi) \end{array} \right\} \quad (27)$$

**Fig. 9** Deformation diagrams,  
a PSBFEM, b NPSBFEM



where the load vector  $\mathbf{q}(\xi)$  is

$$\mathbf{q}(\xi) = \left( \mathbf{E}_0 \xi u(\xi)_{,\xi} + \mathbf{E}_1^T u(\xi) \right) |_{\xi=1} \quad (28)$$

and the Hamiltonian matrix  $\mathbf{Z}$  is defined as

$$\mathbf{Z} = \begin{bmatrix} -\mathbf{E}_0^{-1} \mathbf{E}_1^T & \mathbf{E}_0^{-1} \\ \mathbf{E}_2 - \mathbf{E}_1 \mathbf{E}_0^{-1} \mathbf{E}_1^T & \mathbf{E}_1 \mathbf{E}_0^{-1} \end{bmatrix} \quad (29)$$

By Schur decomposition [47], can be obtained

$$\mathbf{ZV} = \mathbf{ZS} \quad (30)$$

where the Schur matrix  $\mathbf{S}$  and the transformation  $\mathbf{V}$  can be expressed as

$$\mathbf{S} = \begin{bmatrix} \mathbf{S}_n \\ \mathbf{S}_p \end{bmatrix}, \mathbf{V} = \begin{bmatrix} \mathbf{V}_u & \overline{\mathbf{V}}_u \\ \mathbf{V}_q & \overline{\mathbf{V}}_q \end{bmatrix} \quad (31)$$

where  $\mathbf{S}_n$  and  $\mathbf{S}_p$  are the upper triangular matrices corresponding to the negative and positive real parts of the eigenvalues of Hamiltonian matrix  $\mathbf{Z}$ ;  $\mathbf{V}_u$ ,  $\mathbf{V}_q$  and  $\overline{\mathbf{V}}_u$ ,  $\overline{\mathbf{V}}_q$  are modal displacements and modal forces in finite and infinite domains respectively. For a finite field problem, a finite displacement occurs only at the center of scale,  $\mathbf{u}(\xi)$  can be expressed as

$$\mathbf{u}(\xi) = \mathbf{V}_u \eta^{-\mathbf{S}_n} \mathbf{c} \quad (32)$$

where  $\mathbf{c}$  is the integral constant dependent on the boundary conditions. Based on node displacement  $\mathbf{u}_b = \mathbf{u}(\xi = 1)$ , the integral constant can be expressed as

$$\mathbf{c} = \mathbf{V}_u^{-1} \mathbf{u}_b \quad (33)$$

The boundary node force is

$$\mathbf{q}(\xi) = \mathbf{V}_q \mathbf{c} \quad (34)$$

Therefore, the stiffness matrix of the boundary element is

$$\mathbf{k} = \mathbf{V}_q \mathbf{V}_u^{-1} \quad (35)$$

Furthermore, the stiffness matrix of internal polygon elements can be directly solved by the PSBFEM.

### 4.3 The flowchart of NPSBFEM implementation

Firstly, the initial design domain is defined and relevant parameters are provided, including Delaunay triangulation related parameters, loads, boundary conditions, material properties, etc. Secondly, constructing NURBS-boundary-based polygon mesh through NURBS updating strategy and mesh generation scheme discussed in Sect. 2. Next, the stiffness matrices are solved using PSBFEM and NPSBFEM followed by conducting finite element analysis accordingly. Finally, polygon scaled boundary finite element method using NURBS boundary is implemented to obtain the required displacement and stress information. The flowchart of NPSBFEM implementation is shown in Fig. 5.

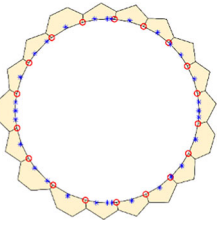
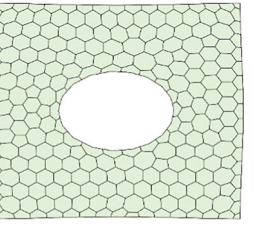
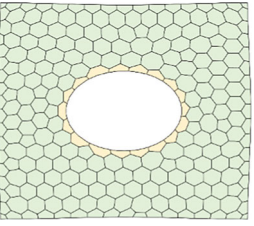
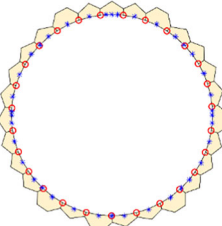
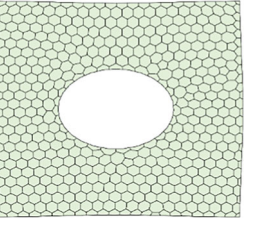
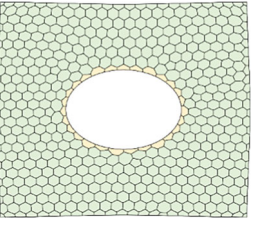
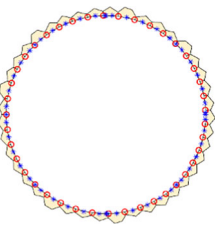
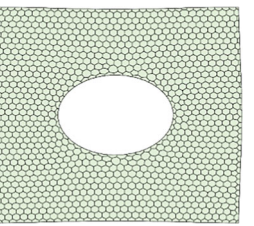
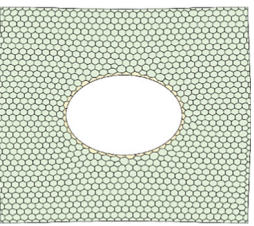
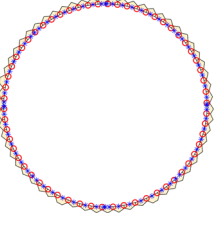
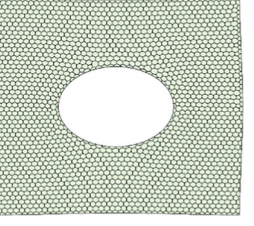
## 5 Examples

In this section, we verify the feasibility of the NURBS-boundary-based polygon mesh generation scheme using NURBS boundary and the effectiveness of NPSBFEM through three examples, including infinite plane with hole, hook structure and serpentine beam. Computations are performed on a PC with 12th Gen Intel(R) Core (TM) i7-12700F 2.10 GHz CPU and 32 GB RAM.

### 5.1 Example 1

The primary objective of this example is to investigate the feasibility of the proposed polygon mesh scheme and NPSBFEM, while also providing a comparative demonstration

**Table 1** The updated control points and the displacement deformation diagrams

| Element numbers | Control points distribution                                                         | PSBFEM                                                                               | NPSBFEM                                                                               |
|-----------------|-------------------------------------------------------------------------------------|--------------------------------------------------------------------------------------|---------------------------------------------------------------------------------------|
| 247             |    |    |    |
| 517             |    |    |    |
| 1197            |    |    |    |
| 2314            |  |  |  |

with traditional polygon mesh and PSBFEM. As shown in Fig. 6, an infinite plane with hole under remote uniaxial uniform tension  $f = 1$  N is employed. The hole with a radius of 0.4 mm is described by NURBS curve. The control points (red points) at [0.4 0; 0.4 0.4; 0 0.4; -0.4 0.4; -0.4 0; -0.4 -0.4; 0 -0.4; 0.4 -0.4; 0.4 0] (mm). The knot vector is [0 0 0 1/4 1/4 2/4 2/4 3/4 3/4 1 1 1], the weights are [ $\sqrt{2}/2$  1  $\sqrt{2}/2$  1  $\sqrt{2}/2$  1  $\sqrt{2}/2$  1], and the degree of NURBS is set to 2. The elastic modulus is specified as 1000 MPa, and Poisson's ratio is 0.25.

The utilization of a  $2 \times 2$  square instead of an infinite plane is employed to model the area surrounding the hole. The exact solution for displacement is specified as the boundary conditions for all four sides of the square. In polar coordinates  $(\rho, \theta)$  [48], the exact solution for this problem is provided as follows

$$\begin{aligned} u_x &= \frac{fr}{8\tau} \left[ \frac{\beta}{r} (1 + \kappa) \cos \theta + \frac{2r}{\beta} ((1 + \kappa) \cos \theta + \cos 3\theta) - \frac{2r^3}{\beta^3} \cos 3\theta \right] \\ u_y &= \frac{fr}{8\tau} \left[ \frac{\beta}{r} (\kappa - 3) \sin \theta + \frac{2r}{\beta} ((1 - \kappa) \sin \theta + \sin 3\theta) - \frac{2r^3}{\beta^3} \sin 3\theta \right] \end{aligned} \quad (36)$$

where  $\tau$  represents the shear modulus, and  $\kappa$  is Kolosov constant defined as

$$\kappa = \begin{cases} \frac{3-\nu}{1+\nu} & \text{for plane stress} \\ 3 - 4\nu & \text{for plane strain} \end{cases} \quad (37)$$

where  $\nu$  is the Poisson's ratio and is set to 0.25. And Young's modulus is defined as 1000 MPa.

When the number of polygon elements is 113, the Distmesh-based polygon mesh with linear elements is shown in Fig. 7a, and Fig. 7b displays the corresponding NURBS-

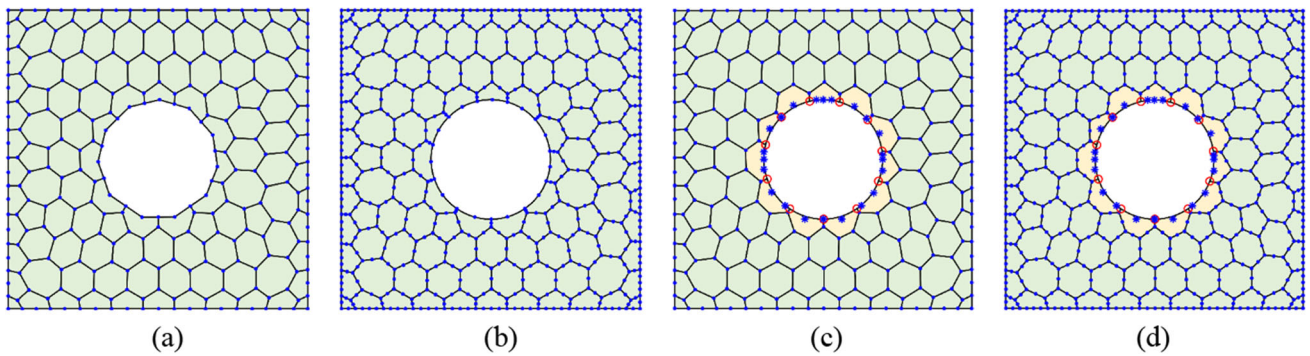


**Fig. 10** The structure diagrams with nodes/control points under **a** linear, **b** quadratic, **c** NURBS + linear, **d** NURBS + quadratic

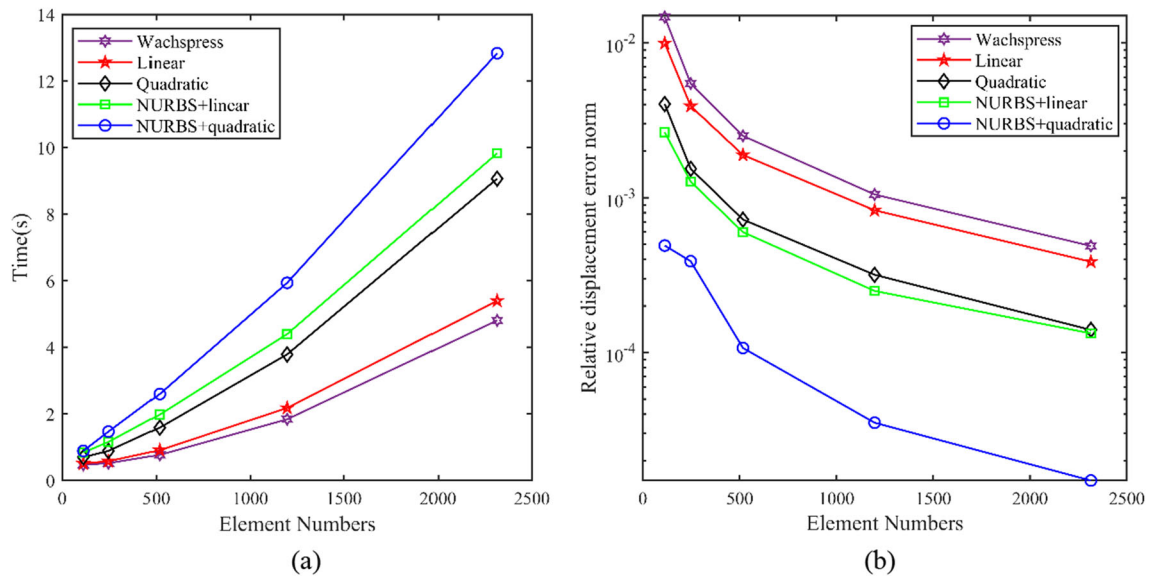


**Fig. 11** The comparison curves between wachspress, linear, quadratic, NURBS + linear and NURBS + quadratic of, **a** time **b** relative displacement error norm

**Table 2** The degrees of freedom and the processing time under different element numbers

| Element numbers | DOFs       |        |           |                |                   | Time(s)    |        |           |                |                   |
|-----------------|------------|--------|-----------|----------------|-------------------|------------|--------|-----------|----------------|-------------------|
|                 | Wachspress | Linear | Quadratic | NURBS + linear | NURBS + quadratic | Wachspress | Linear | Quadratic | NURBS + linear | NURBS + quadratic |
| 113             | 560        | 560    | 1302      | 584            | 1324              | 0.47       | 0.51   | 0.70      | 0.84           | 0.89              |
| 247             | 1154       | 1154   | 2730      | 1178           | 2752              | 0.52       | 0.58   | 0.89      | 1.16           | 1.47              |
| 517             | 2314       | 2314   | 5554      | 2338           | 5576              | 0.77       | 0.91   | 1.59      | 1.98           | 2.60              |
| 1197            | 5162       | 5162   | 12,544    | 5186           | 12,576            | 1.84       | 2.18   | 3.79      | 4.40           | 5.94              |
| 2314            | 9786       | 9786   | 23,960    | 9808           | 23,982            | 4.81       | 5.40   | 9.07      | 9.83           | 12.84             |

boundary-based polygon mesh, which internal elements adopt linear element.

The feasibility of the proposed polygon mesh generation scheme with exact boundary description is clearly evident. While linear segments comprise the boundaries of a polygon

mesh, resulting in rough edges with only  $C^0$  continuity at nodes, the NURBS-boundary-based polygon mesh retains circular characteristics and exhibits smoothness. Figure 8 demonstrates the updated control points constructed by the NURBS updating strategy, while solving for polygon

**Table 3** The relative displacement error norm under different element numbers

| Element numbers | Wachspress | Linear    | Quadratic | NURBS + linear | NURBS + quadratic |
|-----------------|------------|-----------|-----------|----------------|-------------------|
| 113             | 1.47e - 2  | 9.96e - 3 | 4.03e - 3 | 2.65e - 3      | 4.91e - 4         |
| 247             | 5.47e - 3  | 3.91e - 3 | 1.54e - 3 | 1.27e - 3      | 3.89e - 4         |
| 517             | 2.51e - 3  | 1.89e - 3 | 7.23e - 4 | 6.0e - 4       | 1.07e - 4         |
| 1197            | 1.05e - 3  | 8.30e - 4 | 3.18e - 4 | 2.5e - 4       | 3.52e - 5         |
| 2314            | 4.88e - 4  | 3.86e - 4 | 1.40e - 4 | 1.33e - 4      | 1.49e - 5         |

**Table 4** The relative von-Mises stress error norm under different element numbers

| Element Numbers | Linear    | Quadratic | NURBS + linear | NURBS + quadratic |
|-----------------|-----------|-----------|----------------|-------------------|
| 113             | 1.65e - 1 | 1.36e - 1 | 6.33e - 2      | 5.49e - 2         |
| 247             | 8.90e - 2 | 7.62e - 2 | 5.27e - 2      | 4.09e - 2         |
| 517             | 5.21e - 2 | 4.49e - 2 | 3.78e - 2      | 2.62e - 2         |
| 1197            | 2.68e - 2 | 2.40e - 2 | 1.84e - 2      | 1.60e - 2         |
| 2314            | 1.60e - 2 | 1.50e - 2 | 1.33e - 2      | 1.06e - 2         |

elements on the NURBS boundary can be achieved through our proposed NPSBFEM method. Figure 9 illustrates the corresponding structural deformation diagrams for both approaches. It should be noted that the displacement amplification factor is set to 100.

When the elements numbers are 247, 517, 1197, and 2314 respectively, the displacement deformation diagrams and updated control points are presented in Table 1.

The results presented in Table 1 demonstrate the capability of the NPSBFEM to achieve accurate analysis solutions,

regardless of changes in the number of polygons. This validates its exceptional applicability and consistent generation of smooth boundaries. Additionally, the distribution of control points indicates the feasibility of an NURBS updating strategy, eliminating the need for manual provision of new NURBS curves. Furthermore, refinement of the mesh leads to a smoother profile for the inner boundary in PSBFEM.

To verify the accuracy and efficiency of NPSBFEM, four cases are considered: PSBFEM with linear elements, PSBFEM with quadratic elements, NPSBFEM with NURBS + linear elements, and NPSBFEM with NURBS + quadratic elements. Figure 10 illustrates the corresponding structure diagrams containing nodes/control points when there are 113 polygon elements.

The relative displacement error norm  $N_{rde} = \|\mathbf{u}^{exa} - \mathbf{u}^h\| / \|\mathbf{u}^{exa}\|$  is employed to verify the validity of NPSBFEM, where  $\mathbf{u}^{exa}$  and  $\mathbf{u}^h$  respectively represent the analytical solution and the numerical solution. Using 5 different element numbers to discretize the domain, the results between the element numbers, the degrees of freedom (DOFs), and the processing time with Linear, Quadratic, NURBS + linear and NURBS + quadratic under the PSBFEM and NPSBFEM are displayed in Table 2. In addition, the Wachspress interpolation, which is commonly used for polygon elements solving, is introduced for comparison. Table 3 shows the relative displacement error norm ( $N_{rde}$ ) with Wachspress, Linear, Quadratic, NURBS + linear and NURBS + quadratic under different element numbers. And Fig. 11a and b exhibit the corresponding comparison curves of Time and relative displacement error norm.

It is evident that as the number of elements increases, the processing time for all five cases also increases. The

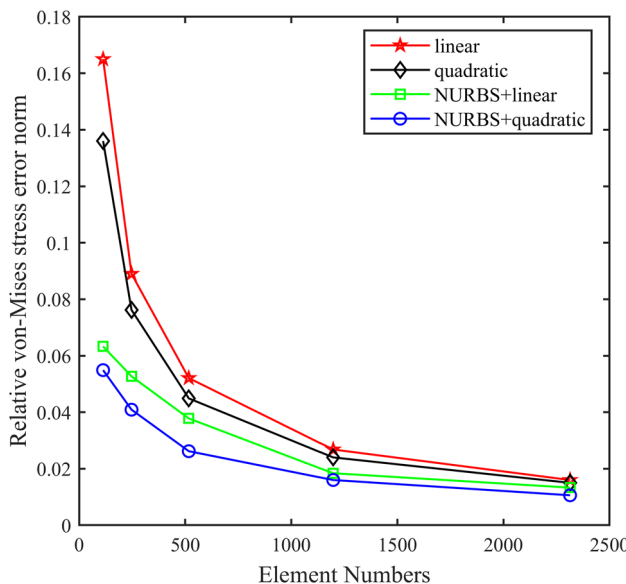


**Fig. 12** The relative von-Mises stress error norm comparison curves between linear, quadratic, NURBS + linear and NURBS + quadratic

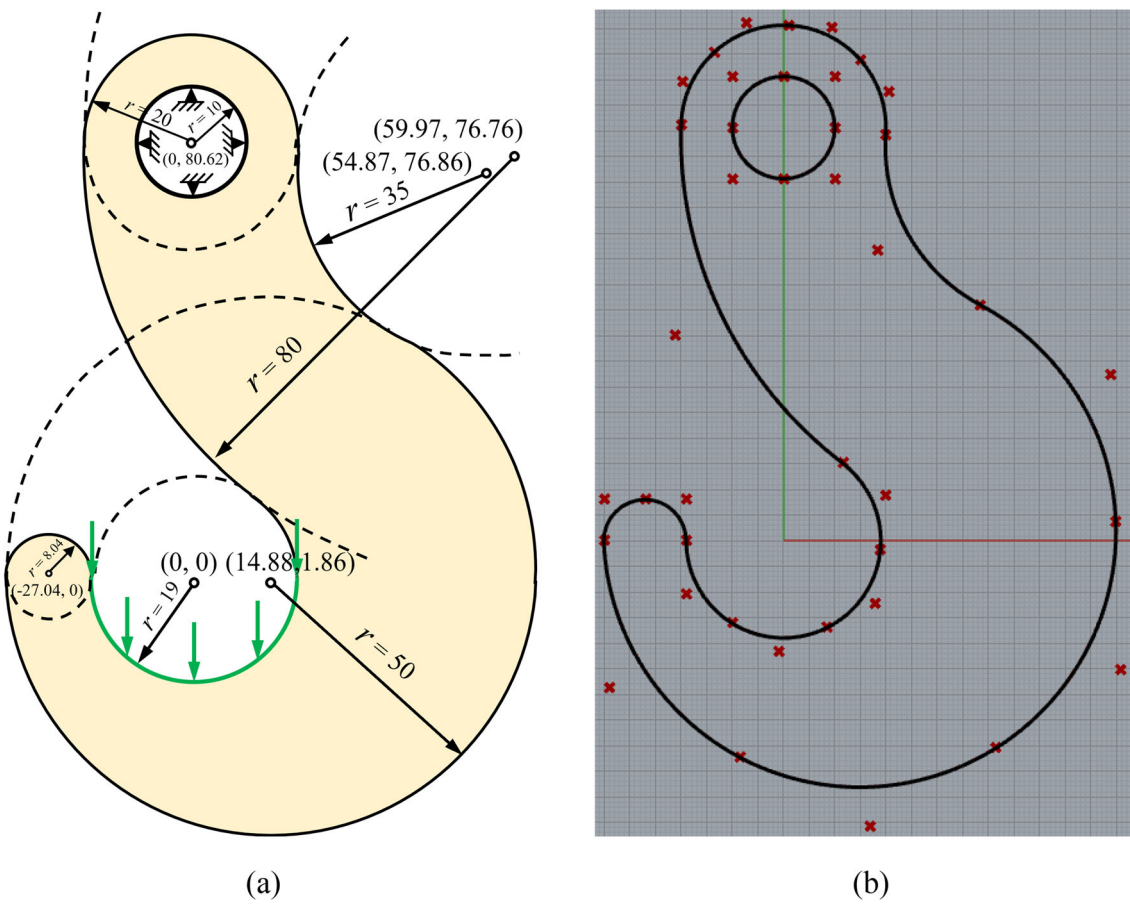


**Fig. 13** The hook structure, **a** sizes, loads and constraints, **b** control points

cases of NURBS + Linear and NURBS + Quadratic exhibit higher time consumption compared to the cases of linear and quadratic, primarily due to the slightly more complex mesh construction involved in the former and the interpolation of boundaries using NURBS.

From the perspective of accuracy, NPSBFEM shows superior accuracy with similar degrees of freedom. Combining Tables 2, 3 and Fig. 11, it is observed that the accuracies of displacement solutions with NPSBFEM are respectively improved by 72.7%–81.6%, 65.5–73.4% and 74.7–89.3% compared with Wachspress and PSBFEM, when contrastively considering the cases of (Wachspress, NURBS + linear), (Linear, NURBS + linear), and (Quadratic, NURBS + quadratic) under similar degrees of freedom. From the perspective of efficiency, the NPSBFEM still demonstrates superior efficiency with similar degrees of freedom. For the case with 5186 DOFs, NPSBFEM of NURBS + linear achieves better  $N_{rde}$  than PSBFEM of linear with 9786 DOFs, and the computational time of former is reduced by 29.8% compared to the latter. Analogously For the case with 5576 DOFs, NPSBFEM of NURBS + linear achieves better  $N_{rde}$  than PSBFEM of linear with 23,960 DOFs,

and the computational time of former is reduced by 71.3% compared to the latter. In other words, NPSBFEM can achieve higher computational accuracy with fewer DOFs, which is an accurate and efficient method.

Simultaneously, to investigate the performance benefits of the proposed approach in relation to stress, the stress analytical solution is expressed in the polar coordinates as

$$\begin{aligned}\sigma_x &= \frac{f}{2} \left( 2 - \frac{r^2}{\beta^2} \left( 3 \cos 2\theta + \left( 2 - \frac{3r^2}{\beta^2} \right) \cos 4\theta \right) \right) \\ \sigma_y &= -\frac{fr^2}{2\beta^2} \left( \cos 2\theta - \left( 2 - \frac{3r^2}{\beta^2} \right) \cos 4\theta \right) \\ \tau_{xy} &= -\frac{fr^2}{2\beta^2} \left( \sin 2\theta + \left( 2 - \frac{3r^2}{\beta^2} \right) \sin 4\theta \right)\end{aligned}\quad (38)$$

In the Cartesian plane coordinate system, the corresponding von-Mises stress is defined as

$$\sigma_e = \sqrt{(\sigma_x + \sigma_y)^2 - 3(\sigma_x \sigma_y) - \tau_{xy}^2} \quad (39)$$

Subsequently, we construct a relative von-Mises stress error norm, formulated as  $N_{rve} = \|\boldsymbol{\sigma}^{exa} - \boldsymbol{\sigma}^h\| / \|\boldsymbol{\sigma}^{exa}\|$ ,

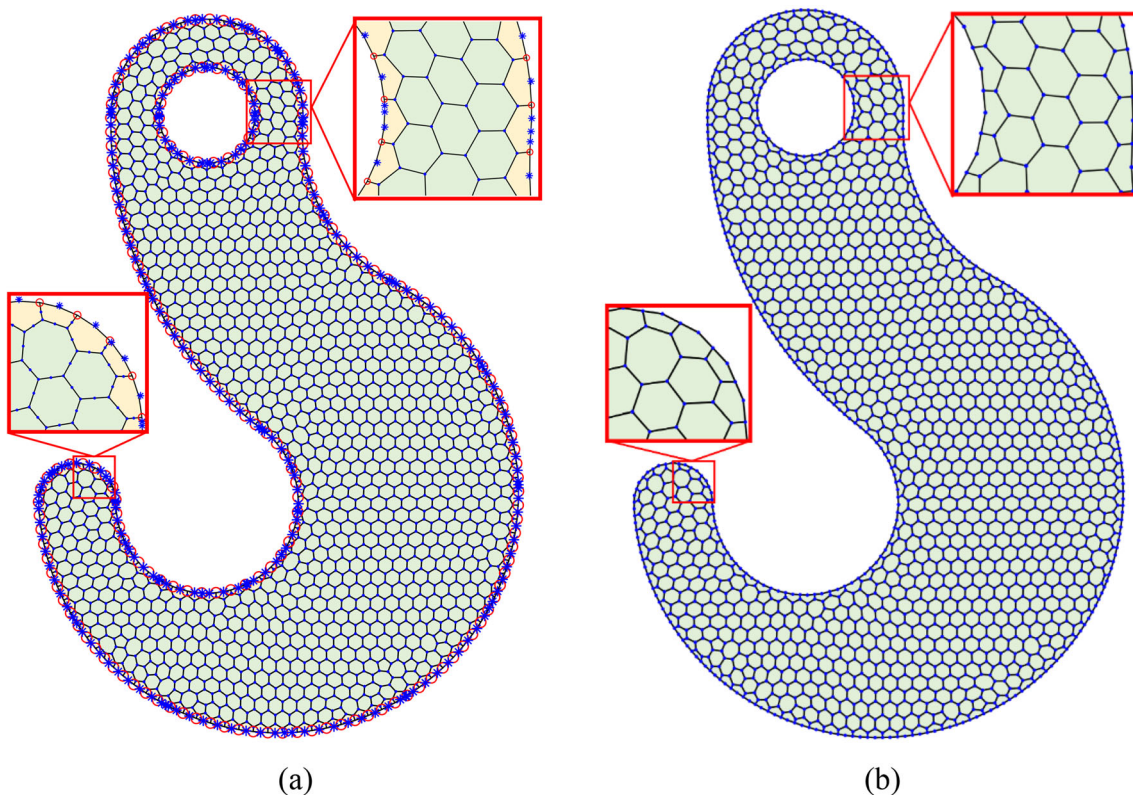


**Fig. 14** The polygon mesh of hook structure, **a** NURBS-boundary-based, **b** Distmesh-based

where  $\sigma^{\text{exa}}$  and  $\sigma^h$  respectively represent the analytical solution and the numerical solution, to further explore the validity of NPSBFEM.

Furthermore, Table 4 shows the relative von-Mises stress error norm ( $N_{\text{rve}}$ ) with Linear, Quadratic, NURBS + linear and NURBS + quadratic under different element numbers. The corresponding comparison curves of  $N_{\text{rve}}$  are displayed in Fig. 12.

Combining with Table 4 and Fig. 12, it can also be observed that NPSBFEM still has a great advantage over PSBFEM in stress performance. With similar degrees of freedom, the accuracy of stress solution is improved by 16.9–61.6% and 29.3–59.6% respectively, when contrastively considering the cases of (Linear, NURBS + linear), and (Quadratic, NURBS + quadratic).

Furthermore, upon comparing the NPSBFEM of NURBS + linear with the PSBFEM of quadratic, it becomes apparent that the latter demonstrates inferior performance in terms of displacement and stress, despite employing quadratic elements within its interior. This disparity primarily arises from the inherent limitations associated with Distmesh's polygon mesh construction, which fails to accurately represent curved boundaries. Conversely, this also underscores the necessity for developing a novel type of polygon mesh capable of accurately describing domain boundaries.

## 5.2 Example 2

This example is mainly intended to validate the applicability of the proposed polygon mesh generation scheme and NPSBFEM for complex design domain. The top circular ring of hook structure internally is fixed, and the semi-arc of bottom part exerts a downward force with a size of 1N. The size and other information of the design domain are shown in Fig. 13a. Figure 13b shows the control points' information of the design domain boundary extracted using Rhino software. The initial information of the NURBS for the hook structure can be found in Appendix A. The degree of NURBS is all set to 2. The elastic modulus is specified as 1000 Mpa, and Poisson's ratio is 0.25.

When the number of elements is set to 1037, Fig. 14a illustrates the NURBS-boundary-based polygon mesh with control points. For comparison, a commonly used Distmesh-based polygon mesh with an equivalent number of elements is introduced, as shown in Fig. 14b. It can be observed from the figure that the proposed mesh generation scheme enables complex design domain structures to be accurately divided into meshes. Due to the introduction of NURBS curves at the boundary, the description of the design domain boundary is smoother and more rational compared to conventional polygon mesh generation schemes which employ linear connections resulting in relatively rough boundaries.

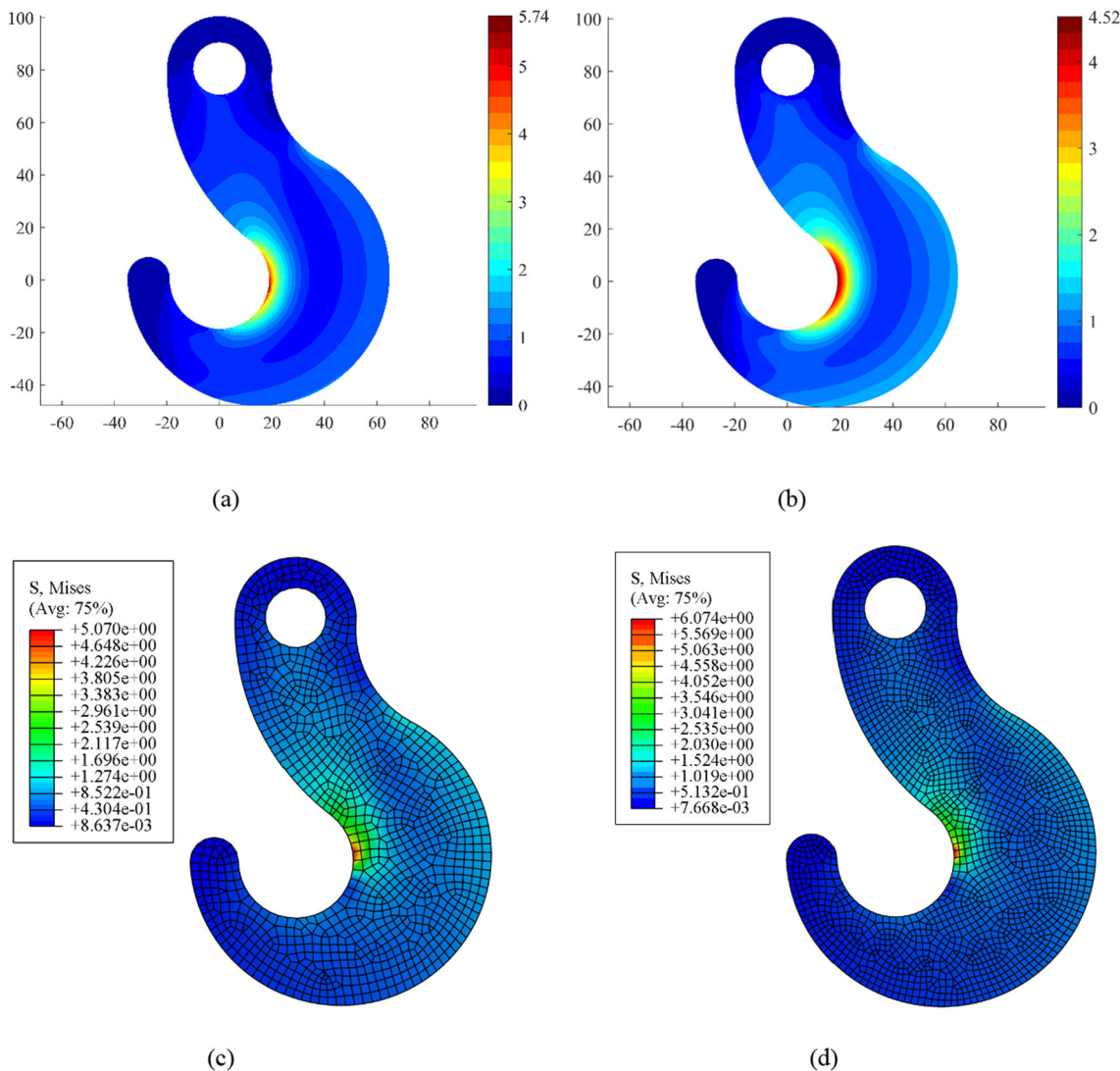


**Fig. 15** The von-Mises stress distribution diagram, **a** NPSBFEM with 1037 elements, **b** PSBFEM with 1037 elements, **c** FEM with 1067 elements, **d** FEM with 1950 elements

Additionally, our proposed spline updating scheme facilitates updates of NURBS and ensures precise alignment between control points and boundary element nodes for subsequent accurate solutions.

In order to investigate the applicability of NPSBFEM in complex design domains, we analyze the von-Mises stress distribution of the hook structure using NPSBFEM (NURBS + linear) and the von-Mises stress obtained from PSBFEM of linear, as shown in Fig. 15a and b. For comparison, the von-Mises stress distributions under finite element software with 1067 and 1950 elements respectively are illustrated in Fig. 15c and d. The results demonstrate that NPSBFEM enables stress analysis in complex design domains. The stress distribution diagram reveals that the maximum stress value (5.74 MPa) achieved by NPSBFEM with 1037 elements surpasses that of PSBFEM (4.52 MPa) with 1037 elements and

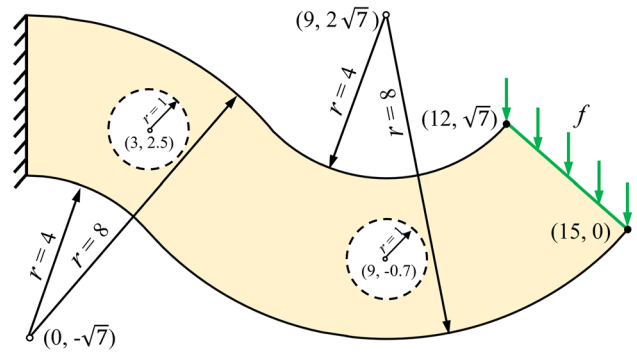


**Fig. 16** The serpentine beam and its size information

FEM (5.07 MPa) with 1067 elements, and is closer to the FEM (6.07 MPa) with 1950 elements. This is attributed

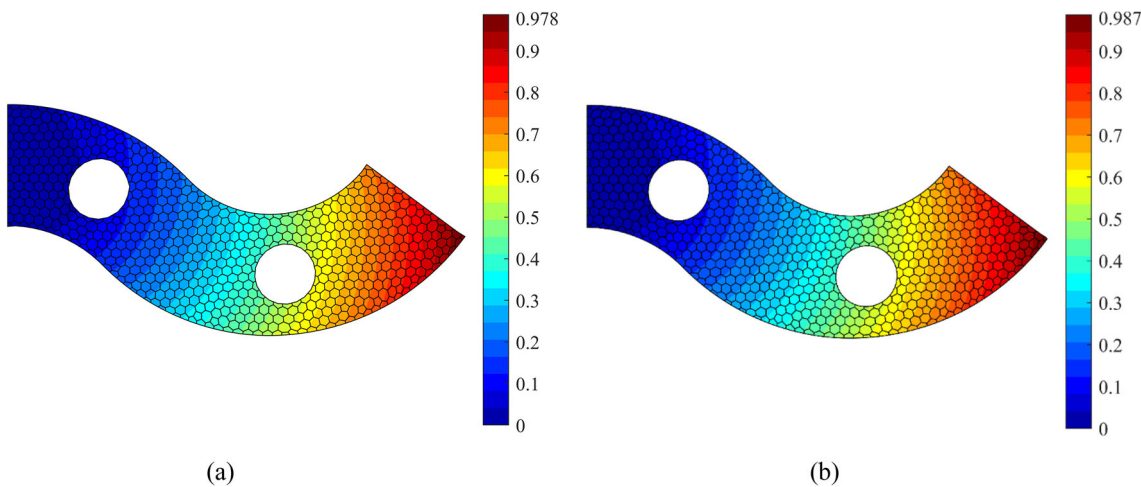


**Fig. 17** Displacement diagrams with mesh distribution, **a** PSBFEM with 712 elements **b** NPSBFEM with 712 elements

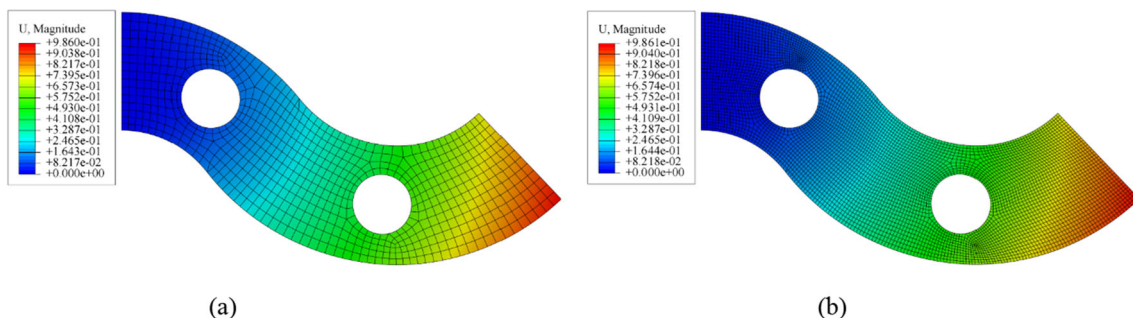


**Fig. 18** Displacement diagrams of finite element software, **a** 770 elements, **b** 5509 elements

to the utilization of higher-order elements at the boundaries, emphasizing the superior performance of NPSBFEM in stress analysis.

### 5.3 Example 3

This example provides a serpentine beam with two circle holes to measure the accuracy of the NPSBFEM, which employs NURBS for the boundary and quadratic elements for the interior. In addition, PSBFEM and finite element software are utilized for comparative analysis. It should be noted that the comparison is predicated on quadratic elements. The structural design domain and size information are shown in Fig. 16. The NURBS information for the serpentine beam with circle holes can be found in Appendix B. The degree of NURBS is set to 2. The left end of the beam is fixed, and the right end is applied a downward uniform load of 1 N. The modulus of elasticity is specified as 1000 MPa and Poisson's ratio is set at 0.25.

When the design domain is discrete to 712 polygon elements under both NPSBFEM and PSBFEM, Fig. 17 displays the displacement diagram with mesh distribution. Figure 18a and b show the displacement diagrams when the number of

elements is 770 and 5509 under the finite element software, respectively. It can be observed that the displacement diagrams obtained through finite element software are relatively stable, with a maximum displacement of 0.986 mm. In contrast, the maximum displacement under NPSBFEM (NURBS + quadratic) is 0.987 mm, which is closer to 0.986 mm compared to the maximum displacement of 0.978 mm under PSBFEM (quadratic). Furthermore, Figs. 19 and 20 depict the corresponding von-Mises stress diagrams to Figs. 17 and 18, respectively. And Table 5 presents the associated values for maximum displacement and maximum stress. From the perspective of stress, the maximum stress obtained with traditional PSBFEM using 712 elements is not as good as that of the FEM with 770 elements, but the maximum stress obtained by NPSBFEM with fewer elements (712) exceeds that of FEM with 770 elements and even approaches the stress values obtained by FEM with more elements (5509). The above results indicate that NPSBFEM can achieve higher accuracy with fewer mesh division.

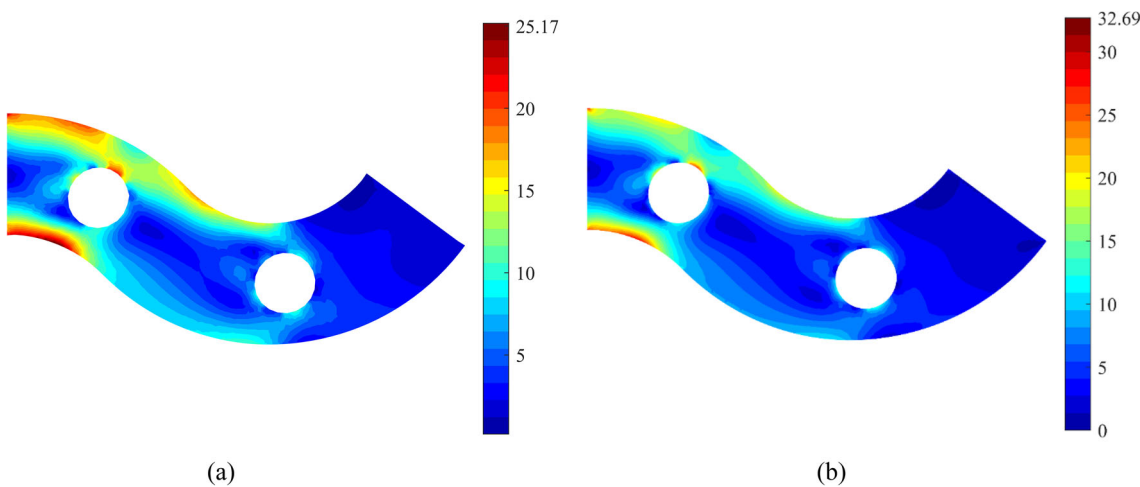


**Fig. 19** Von-Mises stress diagrams, **a** PSBFEM with 712 elements **(b)** NPSBFEM with 712 elements

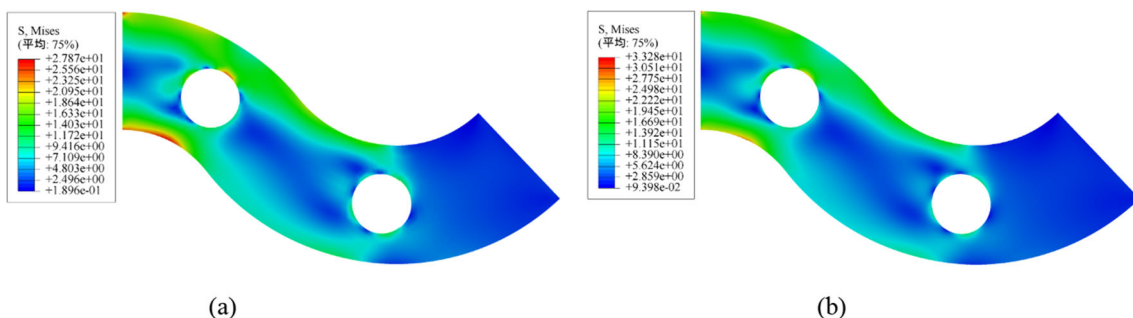


**Fig. 20** Von-Mises stress diagrams of finite element software, **a** 770 elements, and **b** 5509 elements

**Table 5** The maximum displacement and maximum stress of PSBFEM, NPSBFEM and FEM

| Methods                   | PSBFEM (712) | NPSBFEM (712) | FEM (770) | FEM (5509) |
|---------------------------|--------------|---------------|-----------|------------|
| Maximum displacement (mm) | 0.978        | 0.987         | 0.9860    | 0.9861     |
| Maximum stress (MPa)      | 25.17        | 32.59         | 27.87     | 33.28      |

## 6 Conclusions

In this study, a polygon mesh generation scheme using NURBS boundary is proposed, which enables updating of NURBS. Simultaneously, a corresponding polygon scaled boundary finite element method using NURBS boundary, named NPSBFEM, is presented to solve the NURBS boundary element. The numerical examples demonstrate that the polygon mesh generation scheme significantly enhances the quality of a Delaunay-triangulation-based polygon mesh, leading to improved displacement and stress solutions while holding great potential for reducing mesh division costs. Moreover, utilizing NURBS boundaries allows for accurate representation of complex design domains and offers greater flexibility for mesh division in intricate geometric shapes. Furthermore, this method exhibits promising potential in

addressing challenges such as nonlinear problems, fracture mechanics and dynamic simulations.

## Appendix A: NURBS information of hook structure

The control points of the outer boundary are [38.383236, 45.994334; 63.842778, 32.438415; 64.853493, 3.612564; 65.864209, – 25.213286; 41.41664, – 40.519089; 16.969072, – 55.824893; – 8.519635, – 42.323892; – 34.008343, – 28.822891; – 35.0812, 0.000713; – 35.080487, 8.040957; – 27.040243, 8.0406; – 19, 8.040243; – 19, 0; – 19, – 10.570689; – 10.018098, – 16.144279; – 1.036197, – 21.71787; 8.435549, – 17.024737; 17.907295, – 12.331604; 18.913698, – 1.808933; 19.920102, 8.713739; 11.509645, 15.117151;

— 21.263493, 40.069425; — 19.990466, 81.240701; — 19.731193, 89.626057; — 13.567317, 95.317109; — 7.403442, 101.00816; 0.975928, 100.598785; 9.355297, 100.18941; 14.93507, 93.924623; 20.514842, 87.659835; 19.955498, 79.289139; 18.384244, 56.637017; 38.429167, 45.969847](mm). The knot vector is [0 0 0 0.106428 0.106428 0.212856 0.212856 0.319283 0.319283 0.425711 0.425711 0.451401 0.451401 0.47709 0.47709 0.516332 0.516332 0.555574 0.555574 0.594816 0.594816 0.634058 0.634058 0.788801 0.788801 0.821116 0.821116 0.85343 0.85343 0.885745 0.885745 0.918059 0.918059 1 1 1], the weights are [1 0.866205 1 0.866205 1 0.866205 1 0.866205 1 0.707122 1 0.707122 1 0.873862 1 0.873862 1 0.873862 1 0.873862 1 0.88907 1 0.922157 1 0.922157 1 0.922157 1 0.922157 1 0.838919 1].

The control points of the inner boundary are [10, 80.6226; 10, 90.6226; 0, 90.6226; — 10, 90.6226; — 10, 80.6226; — 10, 70.6226; 0, 70.6226; 10, 70.6226; 10, 80.6226]. The knot vector is [0 0 0 1/4 1/4 2/4 2/4 3/4 3/4 1 1 1], the weights are [1 √2/2 1 √2/2 1 √2/2 1 √2/2 1 √2/2 1].

## Appendix B: NURBS information of serpentine beam

The control points of the outer boundary are [0, 5.354249; 0, 3.354249; 0, 1.354249; 1.805665, 1.354249; 3.0, 0; 5.38867, — 2.708497; 9.0, — 2.708497; 12.61133, — 2.708497; 15.0, 0; 13.5, 1.322876; 12.0, 2.645751; 10.805665, 1.291503; 9.0, 1.291503; 7.194335, 1.291503; 6.0, 2.645751; 3.61133, 5.354249; 0, 5.354249] (mm). The knot vector is [0 0 0 0.103815 0.103815 0.191856 0.191856 0.367938 0.367938 0.544021 0.544021 0.647836 0.647836 0.735877 0.735877 0.823918 0.823918 1 1 1], the weights are [1 1 1 0.911438 1 0.911438 1 0.911438 1 0.911438 1 0.911438 1 1].

The control points of the left circle hole are [4 2.5; 4 1.5; 3 1.5; 2 2.5; 2 3.5; 3 3.5; 4 3.5; 4 2.5]. The knot vector is [0 0 0 1/4 1/4 2/4 2/4 3/4 3/4 1 1 1], the weights are [1 √2/2 1 √2/2 1 √2/2 1 √2/2 1 √2/2 1].

The control points of the right circle hole are [10 — 0.7; 10 — 1.7; 9 — 1.7; 8 — 1.7; 8 — 0.7; 8 0.3; 9 0.3; 10 0.3; 10 — 0.7]. The knot vector is [0 0 0 1/4 1/4 2/4 2/4 3/4 3/4 1 1 1], the weights are [1 √2/2 1 √2/2 1 √2/2 1 √2/2 1 √2/2 1].

**Acknowledgements** This work has been supported by National Natural Science Foundation of China [No. 52075184]. This support is gratefully acknowledged.

**Data availability** No data was used for the research described in the article.

## References

- Sukumar N, Tabarraei A (2004) Conforming polygonal finite elements. *Internat J Numer Methods Eng* 61:2045–2066
- Egidi N, Misici L, Piergallini R (2011) PolyFront: an algorithm for fast generation of high quality triangular mesh. *Eng Comput* 27:357–372
- Salinas-Fernández S, Hitschfeld-Kahler N, Ortiz-Bernardin A, Si H (2022) POLYLLA: polygonal meshing algorithm based on terminal-edge regions. *Eng Comput* 38:4545–4567
- Wang H, Qin QH, Lee CY (2019) n-sided polygonal hybrid finite elements with unified fundamental solution kernels for topology optimization. *Appl Math Model* 66:97–117
- Muratov RV, Ryabov PN, Dyachkov SA (2023) Dynamic domain decomposition method based on weighted Voronoi diagrams. *Comput Phys Commun* 290:108790
- Ghosh S, Mallett RL (1994) Voronoi cell finite elements. *Comput Struct* 50:33–46
- Zhang HH, Han SY, Fan LF (2017) Modeling 2D transient heat conduction problems by the numerical manifold method on Wachspress polygonal elements. *Appl Math Model* 48:607–620
- Zhou Y, Zhang Y, Wu J (2023) A polygonal finite volume element method for anisotropic diffusion problemsImage 1. *Comput Math with Appl* 140:225–236
- Belikov VV, Ivanov VD, Kontorovich VK, Korytnik SA, Semenov AY (1997) The non-Sibsonian interpolation: a new method of interpolation of the values of a function on an arbitrary set of points. *Comput Math Math Phys* 37:9–15
- Sukumar N, Malsch EA (2006) Recent advances in the construction of polygonal finite element interpolants. *Arch Comput Methods Eng* 13:129–163
- Meyer M, Barr A, Lee H, Desbrun M (2002) Generalized barycentric coordinates on irregular polygons. *J Graph Tools* 7:13–22
- Floater MS, Kós G, Reimers M (2005) Mean value coordinates in 3D. *Comput Aided Geom Des* 22:623–631
- Song C, Wolf JP (1997) The scaled boundary finite-element method—alias consistent infinitesimal finite-element cell method—for elastodynamics. *Comput Methods Appl Mech Eng* 147:329–355
- Ooi ET, Song C, Tin-Loi F, Yang Z (2012) Polygon scaled boundary finite elements for crack propagation modelling. *Internat J Numer Methods Eng* 91:319–342
- Chiong I, Ooi ET, Song C, Tin-Loi F (2014) Scaled boundary polygons with application to fracture analysis of functionally graded materials. *Internat J Numer Methods Eng* 98:562–589
- Song C (2018) The scaled boundary finite element method: introduction to theory and implementation. Wiley, New Jersey
- Chen D, Dai S (2017) Dynamic fracture analysis of the soil-structure interaction system using the scaled boundary finite element method. *Eng Anal Bound Elem* 77:26–35
- Hu H, Chen D (2023) Uncertainty qualification in evaluating dynamic and static stress intensity factors using SBFEM based on model order reduction. *Eng Fract Mech* 288:109349
- Chidgzey SR, Deeks AJ (2005) Determination of coefficients of crack tip asymptotic fields using the scaled boundary finite element method. *Eng Fract Mech* 72:2019–2036
- Ooi ET, Song C, Tin-Loi F (2014) A scaled boundary polygon formulation for elasto-plastic analyses. *Comput Methods Appl Mech Eng* 268:905–937
- Ye N, Su C, Yang Y (2021) Free and forced vibration analysis in abaqus based on the polygonal scaled boundary finite element method. *Adv Civ Eng* 2021:7664870
- Yang Y, Zhang Z, Feng Y, Wang K (2022) A novel solution for seepage problems implemented in the abaqus UEL based on

- the polygonal scaled boundary finite element method. *Geofluids* 2022:5797014
- 23. Wu S-W, Jiang C, Liu GR, Wan D-T, Jiang C (2022) An n-sided polygonal selective smoothed finite element method for nearly incompressible visco-hyperelastic soft materials. *Appl Math Model* 107:398–428
  - 24. Hughes TJR, Cottrell JA, Bazilevs Y (2005) Isogeometric analysis: CAD, finite elements, NURBS, exact geometry and mesh refinement. *Comput Methods Appl Mech Eng* 194:4135–4195
  - 25. Wang Y, Xiao M, Xia Z, Li P, Gao L (2023) From computer-aided design (CAD) toward human-aided design (HAD): an isogeometric topology optimization approach. *Engineering* 22:94–105
  - 26. Vuong AV, Giannelli C, Jüttler B, Simeon B (2011) A hierarchical approach to adaptive local refinement in isogeometric analysis. *Comput Methods Appl Mech Eng* 200:3554–3567
  - 27. Bazilevs Y, Calo VM, Cottrell JA, Evans JA, Hughes TJR, Lipton S, Scott MA, Sederberg TW (2010) Isogeometric analysis using T-splines. *Comput Methods Appl Mech Eng* 199:229–263
  - 28. Nguyen-Thanh N, Kiendl J, Nguyen-Xuan H, Wüchner R, Bletzinger KU, Bazilevs Y, Rabczuk T (2011) Rotation free isogeometric thin shell analysis using PHT-splines. *Comput Methods Appl Mech Eng* 200:3410–3424
  - 29. Piegl L, Tiller W (1996) The NURBS book. Springer, Heidelberg
  - 30. Zhang Y, Lin G, Hu Z (2010) Isogeometric analysis based on scaled boundary finite element method. *IOP Conf Ser: Mater Sci Eng* 10:012237
  - 31. Lin G, Zhang Y, Hu Z, Zhong H (2014) Scaled boundary isogeometric analysis for 2D elastostatics. *Sci China Phys Mech* 57:286–300
  - 32. Gravenkamp H, Saputra AA, Duczek S (2021) High-order shape functions in the scaled boundary finite element method revisited. *Arch Comput Methods Eng* 28:473–494
  - 33. Zang Q, Bordas SPA, Liu J, Natarajan S (2023) NURBS-Enhanced polygonal scaled boundary finite element method for heat diffusion in anisotropic media with internal heat sources. *Eng Anal Bound Elem* 148:279–292
  - 34. Zang Q, Jansari C, Bordas SPA, Liu J (2024) Trimming with polygonal scaled boundary isogeometric method. *Comput Struct* 295:107270
  - 35. Lin G, Peng Li, Liu J, Zhang P (2017) Transient heat conduction analysis using the NURBS-enhanced scaled boundary finite element method and modified precise integration method. *Acta Mech Solida Sin* 30:445–464
  - 36. Wang W, Peng Y, Wei Z, Guo Z, Jiang Y (2019) High performance analysis of liquid sloshing in horizontal circular tanks with internal body by using IGA-SBFEM. *Eng Anal Bound Elem* 101:1–16
  - 37. Liu J, Li J, Li P, Lin G, Xu T, Chen L (2018) New application of the isogeometric boundary representations methodology with SBFEM to seepage problems in complex domains. *Comput Fluids* 174:241–255
  - 38. Yang YB, Li J (2022) 2.5D prediction of soil vibrations due to railway loads by the isogeometric analysis with scaled boundary. *Eng Anal Bound Elem* 134:341–359
  - 39. Li X, Su H, Yang J, Gao G, Wang Y (2024) NURBS-boundary-based quadtree scaled boundary finite element method study for irregular design domain. *Eng Anal Bound Elem* 159:418–433
  - 40. Klinkel S, Chen L, Dornisch W (2015) A NURBS based hybrid collocation–Galerkin method for the analysis of boundary represented solids. *Comput Methods Appl Mech Eng* 284:689–711
  - 41. Klinkel S, Reichel R (2019) A finite element formulation in boundary representation for the analysis of nonlinear problems in solid mechanics. *Comput Methods Appl Mech Eng* 347:295–315
  - 42. Reichel R, Klinkel S (2023) A non-uniform rational B-splines enhanced finite element formulation based on the scaled boundary parameterization for the analysis of heterogeneous solids. *Internat J Numer Methods Eng* 124:2068–2092
  - 43. Persson P-O, Strang G (2004) A simple mesh generator in MATLAB. *SIAM Rev* 46:329–345
  - 44. Wolf JP, Song C (2000) The scaled boundary finite-element method – a primer: derivations. *Comput Struct* 78:191–210
  - 45. Wolf JP, Song C (2001) The scaled boundary finite-element method – a fundamental solution-less boundary-element method. *Comput Methods Appl Mech Eng* 190:5551–5568
  - 46. Vu TH, Deeks AJ (2006) Use of higher-order shape functions in the scaled boundary finite element method. *Internat J Numer Methods Eng* 65:1714–1733
  - 47. Song C (2004) A matrix function solution for the scaled boundary finite-element equation in statics. *Comput Methods Appl Mech Eng* 193:2325–2356
  - 48. Fries TP (2017) Higher-order meshing of implicit geometries—part III: conformal decomposition FEM (CDFEM). *ArXiv abs/1706.00919*

**Publisher's Note** Springer Nature remains neutral with regard to jurisdictional claims in published maps and institutional affiliations.

Springer Nature or its licensor (e.g. a society or other partner) holds exclusive rights to this article under a publishing agreement with the author(s) or other rightsholder(s); author self-archiving of the accepted manuscript version of this article is solely governed by the terms of such publishing agreement and applicable law.